Improvement of the Representative Volume Element Method for 3-D Scaffold Simulation

Lv-Sha Cheng
Department of Precision Machinery and Precision Instrumentation, University of Science and Technology of China, Hefei, Anhui Province 230026, China
Hyun-Wook Kang, Dong-Woo Cho*
Department of Mechanical Engineering, Pohang University of Science and Technology, San 31, Hyoja dong, Nam-gu, Pohang, Kyungbuk 790-784, Korea

Predicting the mechanical properties of the 3-D scaffold using finite element method (FEM) simulation is important to the practical application of tissue engineering. However, the porous structure of the scaffold complicates computer simulations, and calculating scaffold models at the pore level is time-consuming. In some cases, the demands of the procedure are too high for a computer to run the standard code. To address this problem, the representative volume element (RVE) theory was introduced, but studies on RVE modeling applied to the 3-D scaffold model have not been focused. In this paper, we propose an improved FEM-based RVE modeling strategy to better predict the mechanical properties of the scaffold prior to fabrication. To improve the precision of RVE modeling, we evaluated various RVE models of newly designed 3-D scaffolds using FEM simulation. The scaffolds were then constructed using microstereolithography technology, and their mechanical properties were measured for comparison.

Key Words: Tissue Engineering, Scaffold, RVE Model, FEM, Microstereolithography Technology

Nomenclature

Y : Length scale in Global coordinate system
y : Length scale in Local coordinate system
ε : Scaling parameter
i : The current structural level
$i-1$: The next largest macroscopic level
$[M_i]$: The i-th level of the local structure matrix
$[C_i]$: The stiffness of the i-th structural level
V_{RVE} : RVE (representive volume element) volume
S1 : A surface of RVE model that is fixed in the z-direction
S2 : A surface on which a uniform displacement is applied
E_Z : Effective Young's modulus
A_{S1}, A_{S2} : The areas of surfaces S1 and S2
L_Z : The dimension of the RVE model in the z-direction
F : Reaction force
σ_R : Reaction stress
d : Displacement
λ : Wavelength
R : Gaussian half-width
f : Focal length
$W_{o,\min}$: Gaussian half-width at the focal point

* Corresponding Author,
E-mail : dwcho@postech.ac.kr
TEL : +82-54-279-2171; **FAX** : +82-54-279-5899
Department of Mechanical Engineering, Pohang University of Science and Technology, San 31, Hyoja dong, Nam-gu, Pohang, Kyungbuk 790-784, Korea. (Manuscript **Received** May 11, 2006; **Revised** July 3, 2006)

1. Introduction

A scaffold for cell growth can be tailored to the target tissue prior to implantation (Vacanti and

Langer, 1999). For effective tissue regeneration, the scaffold design should include the following features: a three-dimensional (3-D) and highly porous structure to support cell attachment and proliferation, and extracellular matrix (ECM) production; an interconnected and permeable pore network to promote nutrient and waste exchange; mechanical properties that support or match those of the tissues at the implantation site; an architecture that promotes the formation of the native anisotropic tissue structure; and a reproducible structure of clinically relevant size and shape (Langer and Joseph, 1993; Hollister et al., 2002; Hutmacher, 2000; Landers and Mulhaupt, 2000).

FEM analysis is one of the most powerful tools for simulating a porous scaffold model and predicting its mechanical properties. The method can simulate structural deformation due to stress and strain, making it particularly useful for identifying potentially dangerous areas and fracture risk of the structure. However, the FEM approach is limited when applied to porous structures such as scaffolds. In some cases, the demands of the procedure are too high for a computer to run standard FEM analysis at the pore level. To overcome this limitation and take full advantage of the analytical power of FEM simulation, representative volume element (RVE) theory was introduced to simplify scaffold architecture (Fang and Sun, 2005) and better predict its mechanical properties. RVE has also been used to simulate original tissue, combining RVE-based homogenization with digital imaging to estimate strain at various levels of bone structure (Hollister and Kikuchi, 2005). Thus far, however, studies on the effects of RVE modeling technology on prediction accuracy of the 3-D scaffold design have not been focused.

The objective of this study was to improve the RVE modeling strategy for FEM simulation to better predict the mechanical properties of scaffolds prior to fabrication. The improved strategy was verified by comparing simulation results. The scaffolds were manufactured using microstereolithography and a computer-controlled design and fabrication process, and their mechanical properties were compared.

2. Computer Simulation of the Scaffold

2.1 RVE theory and model design

2.1.1 RVE theory

RVE theory is often applied to analyze heterogeneous structures. The global coordinate system Y and the local coordinate system y are two length scales for body structural analysis (Fang and Sun, 2005), as shown in Fig. 1.

The global length scale in the global coordinate system is proportional to the local length scale of the unit cell in the local coordinate system, and is expressed as follows:

$$Y=\frac{y}{\varepsilon} \tag{1}$$

where ε is a scaling parameter that is always equal to the ratio of unit cell size to the macroscopic region of the global coordinate system in which it belongs. In this equation, the representative section of a structural level defined as RVE is analyzed under assumed boundary conditions to calculate the average or the effective stiffness properties of that section. The prediction values change as the number of repeating units in the local length level of the local coordinate changes, as follows:

$$\varepsilon_i=[M_i]\cdot\varepsilon_{i-1} \tag{2}$$

where i is the current structural level being analyzed, $i-1$ denotes the next largest macroscopic level, and $[M_i]$ is the local structure matrix (Liu and Abramson, 2003). To determine the effective stiffness of the global structure, the stiffness of the local structure can be analyzed. Combining Eqs. (1) and (2), the stiffness of the local structure is

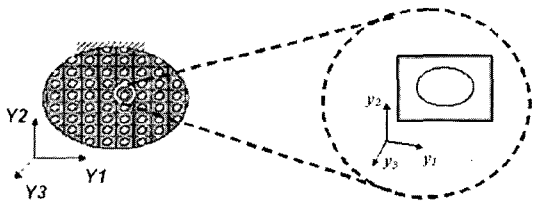

Fig. 1 The global and local coordinate systems

calculated as follows (Liu and Abramson, 2003) :

$$[C_{i-1}]=\frac{1}{V_{RVE}}\cdot\int[C_i][M_i]dV_{RVE} \quad (3)$$

where $[C_{i-1}]$ is the stiffness of the i-1 th structural level, $[C_i]$ is the stiffness of the i-th structural level, V_{RVE} is RVE volume, and $[M_i]$ is the i-th level of the local structure matrix.

The RVE model extracted from the global structural level was defined to represent the typical material of an average structure, and to contain a sufficient number of irregularities or variety in the structure so that the apparent modulus would be independent of the RVE boundary displacements or tractions (Fang and Sun, 2005). In RVE theory, the boundary condition affects prediction precision when applied to RVE models; thus, the more sections included in the RVE model, the less effect boundary conditions will have. In the scaffold simulation process, uniform stress or strain is always added in a certain direction. We may deduce that predictions can be improved by selecting more sections in a particular direction, and reduce sections in other directions to simplify the RVE model.

2.1.2 Model building

The macro- and microstructure of the scaffold are critically important to tissue regeneration. For example, the optimum scaffold pore size is 100-350 μm for the regeneration of bone (Fang and Sun, 2005). With this in mind, we chose a 3-D scaffold model with an overall size of 4×4×4 mm, to provide high porosity for cell attachment and full interconnectivity for waste and nutrition exchange (Fig. 2(a)). As shown in the figure, the model includes thousands of homogeneous, rectangular pores distributed throughout the scaffold. According to RVE theory, the unit RVE model, defined here as a unit pore with appropriate wall thickness, has the same porosity as the whole model (Fig. 2(b)).

In the RVE model-building process, all of the 24 RVE models and 4 scaffold models were built using Unigraphic software. Different numbers of unit RVE models were used to analyze RVE modeling strategies. Each RVE model was described by the number of unit RVE models in the x-y-z directions (Fig. 3, Table 1).

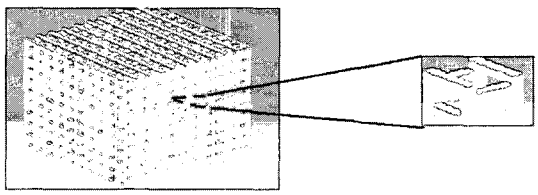

Fig. 2 Whole model and unit RVE model

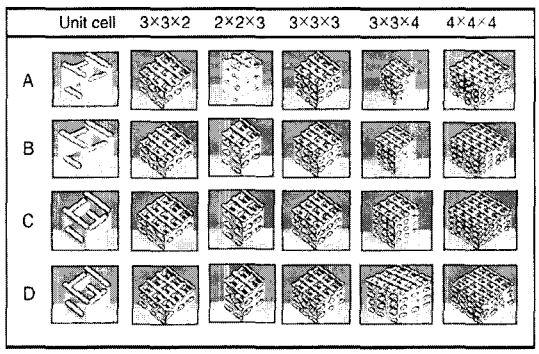

Fig. 3 RVE model designs

Table 1 RVE models

RVE model		Unit cell	2×2×3	3×3×2	3×3×3	3×3×4	4×4×4
RVE shape		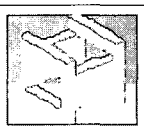			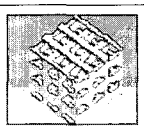	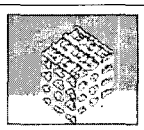	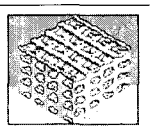
Number of unit models in x,y,z directions	x	1	2	3	3	3	4
	y	1	2	3	3	3	4
	z	1	3	2	3	4	4

Table 2 Scaffold characteristics

No.	Pore Size (um)			Wall thickness (um)	Pore construction in whole model (Pore number in x, y, z directions)	Porosity (%)
	X-direction	Y-direction	Z-direction			
A	180	180	100	80	15×15×20	69.23%
B	200	200	100	80	15×15×20	71.43%
C	230	230	100	80	15×15×20	74.19%
D	250	250	100	80	15×15×20	75.76%

In Fig. 3, A, B, C, and D represent scaffolds with different pore constructions. The parameters of each scaffold characteristic are shown in Table 2.

2.2 FEM analysis and comparison

2.2.1 FEM simulation

To calculate the elastic modulus of the designed model, we used the FEM (ANSYS 10.0) based on elastic theory. For a given structure, commercialized polymer (SL5180; Huntsman International, Salt Lake City, UT) was considered in the simulation process. Then the meshing strategy was applied to generate the appropriate calculating nodes on the scaffold area. The boundary loading condition is shown in Fig. 4. Surface S1 is fixed in the z-direction, and a uniform displacement (d=0.001) is applied on the surface S2.

The effective Young's modulus E_Z can be calculated as follows:

$$E_Z=\frac{\sigma_Z}{\varepsilon_Z}=\frac{\frac{F}{A_{S2}}}{\frac{d}{L_Z}}=1000\times\frac{F\cdot L_Z}{A_{S2}} \tag{4}$$

where A_{S1} and A_{S2} are the areas of surfaces S1 and S2, respectively, L_Z is the dimension of the RVE model in the z-direction, and F and σ_R are the reaction force and stress produced on surface S1 caused by prescribed displacement d on surface S2 determined by Eq. (5).

$$F=\int_{S2}\sigma_R dA \tag{5}$$

After applying the boundary loading, the models

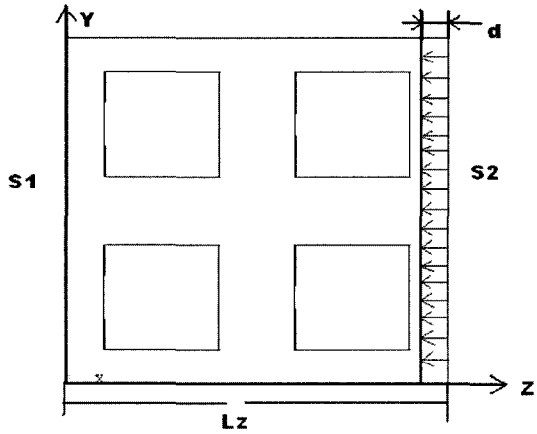

Fig. 4 The loading boundary condition for the RVE

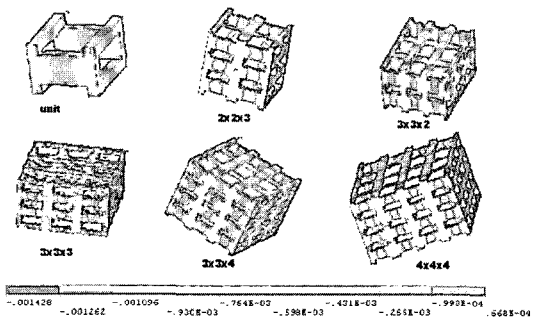

Fig. 5 Strain deformation of various RVE models

are subjected to displacement, and the boundary load. The strain of several models with a pore size of 180 μm are shown in Fig. 5.

2.2.2 Calculation results

After simulating the proposed RVE models, the calculations described above were performed on each of the scaffold models. For each model, the effective Young's modulus was obtained from the FEM simulation. The relationships between pore

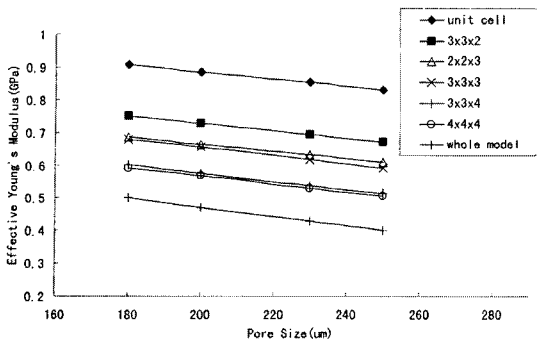

Fig. 6 Simulation results of RVE models for 3-D scaffold

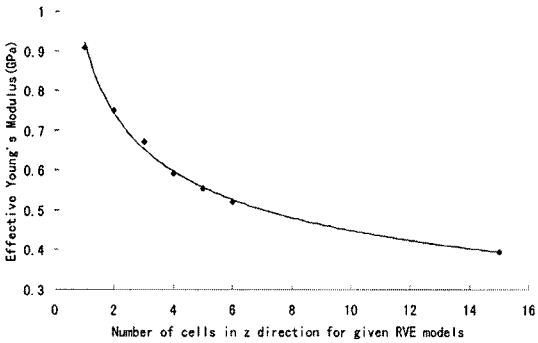

Fig. 7 The length effect in the z-direction

size and effective Young's modulus are shown in Fig. 6.

The effective Young's modulus of models with the same number of unit RVE models in the z-direction have similar results. The Young's modulus of the $3\times3\times4$ and $4\times4\times4$ models, among those proposed in Table 1, have the smallest error (vs. whole model), while that of the unit RVE model has the biggest error. When the pore size of the scaffold increased, the effective Young's modulus decreased in every case.

These results indicate that length in the z-direction tends to determine the precision of the predicted effective Young's modulus, as shown in Fig. 7. The value of simulated effective Young's modulus should not be related to the area of the cross section. Fig. 8 shows the area effect in the RVE modeling. However, when less area was applied to certain displacements, an edge effect was generated by the boundary of the area, as shown by the color differences between the boundary and the rest of the area following strain deformation.

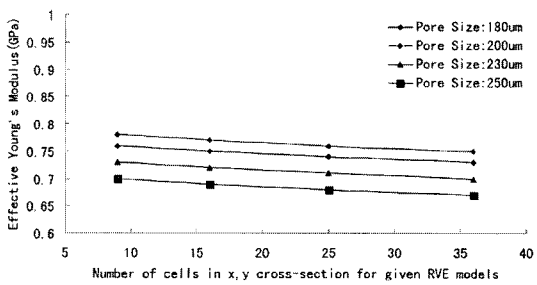

Fig. 8 The area effect in the x-y cross section

Of all the RVE models listed in Table 1, the $3\times3\times4$, $4\times4\times4$, and $5\times5\times4$ models appear to be the most accurate. In terms of model building and simulation time, $3\times3\times4$ is the most appropriate model.

3. Scaffold Fabrication and Experiments

3.1 Microstereolithography system and scaffold fabrication

A number of fabrication technologies have been applied to meet the complex requirements of effective scaffolds (Liu and Abramson, 2003). However, scaffolds built from these methods and used to generate new tissues or tissue substitutes have not functioned satisfactorily. To more precisely fabricate the delicate scaffold, we used a 3-D freedom fabrication system called microstereolithography (Lee and Cho, 2002 ; Kang et al., 2005 ; Lee et al., 2005 ; Lee and Kim, 2005 ; Ikuta and Hirowatari, 1993).

Figure 9 shows a schematic drawing of the microstereolithography apparatus. An Ar^+ laser with a wavelength λ of 351.1 nm and a Gaussian half-width R of 0.85 mm was used as the light source. A neutral density (ND) filter attenuated the power of the laser. Laser beam splitters and mirrors were used to change beam path, and a lens with a focal length f of 50.8 mm focused the beam on the surface of the photopolymer. In our system, the substrate upon which the laser beam was fixed moved in three orthogonal directions (x, y, and z) in the photopolymer container. In microstereolithography, the UV laser beam must be focused to within a few micrometers.

When a focusing lens with a relatively long focal length is used, the Gaussian half-width at the focal point $W_{o,\min}$ increases as:

$$W_{0,\min}=\frac{f\cdot\lambda}{\pi\cdot R} \tag{6}$$

This microstereolithography system, along with commercialized UV curable polymer material (SL 5180), was used to address all the micro and macro requirements for scaffold fabrication. The fabrication parameters were set as follows: laser power of 70 μw, scanning speed of 60 mm/min, and layer thickness of 100 μm. As previously noted, microstereolithography can show the delicate shape of fabricated scaffolds. Fig. 10 presents microscope images of fabricated 3-D scaffolds.

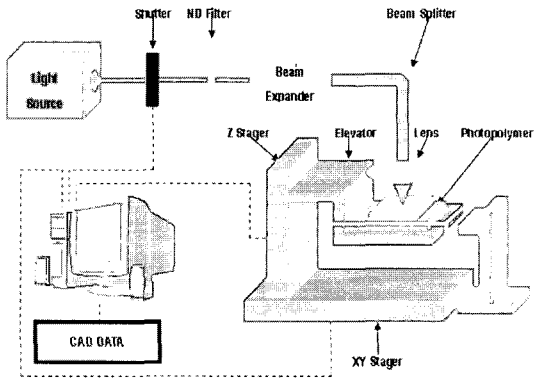

Fig. 9 Schematic drawing of the microstereolithography apparatus

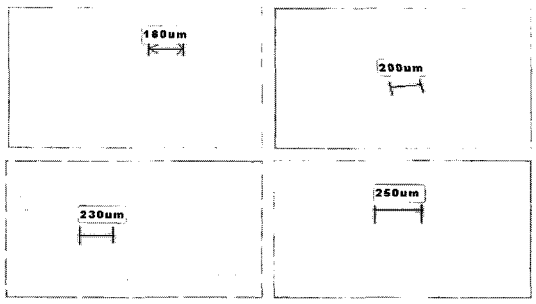

Fig. 10 Microscope images of fabricated 3-D scaffold

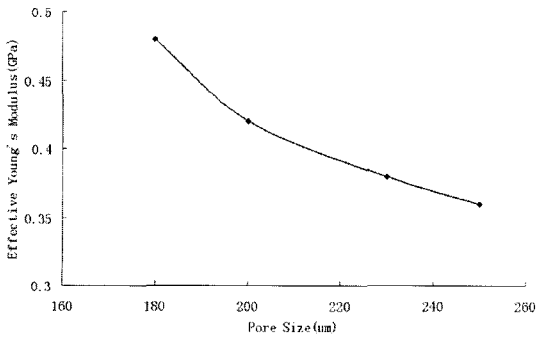

Fig. 11 Scaffold experimental results

3.2 Mechanical testing experiment

A mechanical test was conducted using a Universal testing machine (INSTRON 5582). Imposed displacements and measured loads were normalized to sample thickness and area to yield strains and stress, respectively. The specimens were compressed by sequential increments of strain, at a calculated strain rate of 0.005 m/min, up to a maximum of 15% total strain. Finally, the modulus of samples was calculated from the equilibrium stress-strain curve obtained by linear regression of the data in the region of 0 to 5% strain. The results of this experiment are presented in Fig. 11.

4. Results and Discussion

From the simulation results described earlier, the 3×3×4 model is the best RVE model for scaffold simulation. Fig. 12 compares the experimental and simulation results of the 3×3×4 RVE model and the whole model. The experimental and simulation results showed the same trend, though the experimental results showed some differences. This means that the simulation process was suitable. And, when we know the

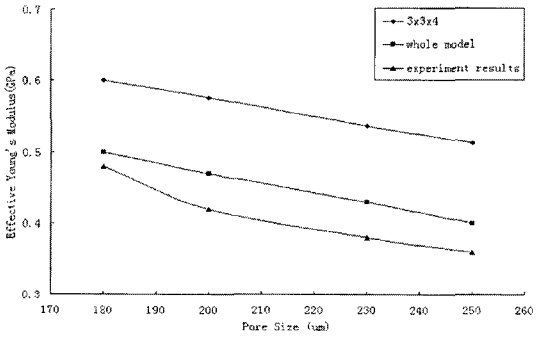

Fig. 12 Comparison between simulation and experiment results

offset error, predication accuracy can be dramatically increased.

5. Conclusions

In this study, we performed both simulations and experiments with scaffold models in virtual and real domains. Different RVE models based on a newly designed 3-D scaffold model were designed to test the improved modeling strategy, which was verified by comparing FEM simulations and experiments. Figs. 6 and 12 show that the effective Young's modulus of models with the same number of unit RVE models in the z-direction have similar results, and that the simulated effective Young's modulus was not related to cross-sectional area. Moreover, the effective Young's modulus of models with high numbers of unit RVE models is closer to that of the whole model. When the pore size of the scaffold increased, the effective Young's modulus decreased in every simulated pore size case. Furthermore, the curve of the experimental results shows the same trend as the curve of the simulation results for the whole model.

As indicated earlier, prediction precision can be improved by increasing the number of unit RVE models in a certain direction and decreasing the number in other directions to simplify the model-building process and reduce simulation time. Therefore, FEM simulations can be improved by applying the proposed RVE modeling strategy.

Acknowledgements

This work was supported by Korea Science & Engineering Foundation through the NRL Program (Grant M10500000042).

References

Fang, Z. and Sun, Wei., 2005, "Computer-aided Characterization for Effective Mechanical Properties of Porous Tissue Scaffold," *Computer-aided Design*, Vol. 37,pp. 65～72.

Fang, Z. and Sun, Wei., 2005, "Homogenization of Heterogeneous Tissue Scaffold : a Comparison of Mechanics, Asymptotic Homogenization, and Finite Element Approach," *J. of Bionics and Biomechanics*, Vol. 2, pp. 17～29.

Hollister, S. J., Maddox, R. D. and Taboas, 2002, "Optimal Design and Fabrication of Scaffolds to Mimic Tissue Properties and Satisfy Biological Constraints," *Biomaterials*, Vol. 23, pp. 95～103.

Hollister, S. J. and Kikuchi, N., 2005, "Homogenization Theory and Digital Imaging : A Basis for Studying the Mechanics and Design Principles of Bone Tissue," *Biotechnology and Bioengineering*, Vol. 43, Issue 7, pp. 586～596.

Hutmacher, D. W., 2000, "Scaffolds in Tissue Engineering Bone and Cartilage," *Biomaterials*, Vol. 21, pp. 29～43.

Ikuta, K. and Hirowatari, K., 1993, "Real Three-dimensional Microfabrication Using Stereo Lithography and metal Molding. In : Proceedings of the IEEE International Workshop on Micro Electro Mechanical Systems (MEMS '93)," *Fort Lauderdale*, FL, 7～10 February 1993, pp. 42～47.

Kang, H.-W., Lee, I. H., Cho, D.-W. and Yun, W. S., 2005, "Development of Micro-bellows Actuator Using Micro-stereolithography Technology," *International Conference on Micro- and Nano-engineering 2005*, 9D_01, Vienna, Austria, September 19-22.

Landers, R. and M.ulhaupt, R., 2000, "Desktop Manufacturing of Complex Objects, Prototypes & Biomedical Scaffolds by Means of Computer-assisted Design Combined with Computer-guided 3D Plotting of Polymers & Reactive Oligomers," *Macrol Mater Eng.*, Vol. 282, pp. 17～21.

Langer, R. and Joseph. P., 1993, "Tissue Engineering," *Science*, Vol. 260, pp. 920～926.

Lee, I. H. and Cho, D.-W., 2002, "Micro-stereolithography Photopolymer Solidification Patterns for Various Laser Beam Exposure Conditions," *International Journal of Manufacturing and Technology*, Vol. 22, pp. 410～416.

Lee, S. J. and Kim, B., 2005, "Development of Three-dimensional Scaffolds Using Micro-stereolithography Technology," *The 8th Annual Meeting of Tissue Engineering Society International*,

Shanghai, China, No. 269, October 22-25.

Lee, S. J., Kang, H. -W., Kim, Y. G. and Cho, D. -W., 2005, "Development of a Micro-blood-typing System Using Micro-stereolithography," *Sensors and Materials*, Vol. 17, No. 3, pp. 113~123.

Liu, Y. and Abramson, S., 2003, "Characterizing the Mechanical Properties of Poly-(Dte CaRbONate) Scaffold from the Finite Element Simulation of its Microtopology," *IEEE Conference*, 22-23 March.

Vacanti, J. P. and Langer, R., 1999, "Tissue Engineering : the Design and Fabrication of Living Replacement Devices for Surgical Reconstruction and Transplantation," *Lancet.*, Vol. 354, pp. 32~34.